Design and Fabrication of CNT-Based *E*-Gun Using Stripe-Patterned Alloy Substrate for X-Ray Applications

Jongmin Lim, Amar P. Gupta, Seung Jun Yeo, Mallory Mativenga, Moonkyoo Kong, Chong-Gil Cho, Jeung Sun Ahn, Seung Hoon Kim, and Jehwang Ryu

***Abstract*— We report the enhancement of carbon nanotube (CNT) field emitters by growing them directly on stripe-patterned alloy substrates. For a gate voltage of 1300 V, CNT field emitters grown on full and stripe-patterned alloy substrates achieved respective emission currents of 0.22 and 2.32 mA, corresponding to tenfold performance enhancement. Performance enhancement is attributed to the reduced screening effect (as a result of the spacing between strips) during field emission and a damage-free patterning process. To verify the ability of the stripe-patterned CNT field emitters to generate X-rays, we designed and assembled an electron gun through brazing. With the open type X-ray system, an X-ray image of human teeth was successfully obtained, verifying the potential of the stipe-patterned CNT emitters in X-ray applications.**

***Index Terms*— Carbon nanotube (CNT), field emission, X-ray.**

I. Introduction

CARBON nanotube (CNT) field emitters have enormous potential in many different areas, particularly in X-ray technology, where CNT-based emitters provide many new possibilities in vacuum electronic devices [1]–[3]. The CNT-based X-ray system has many advantages because of CNT's superior electrical and mechanical characteristics [4]. It is hard to achieve pulsed X-ray radiation with filament X-ray sources based on thermionic emission because of their long response time and high operating temperature. On the contrary, CNT field emitters can be swiftly turned on and off, allowing the generation of the pulsed emission. In addition, electron extraction from CNTs for X-ray radiation is possible at room temperature, allowing the formation of cold cathode X-ray sources [5]–[9]. During the growth of CNTs by chemical vapor deposition (CVD), it is important to select the type of substrate (e.g., silicon or metal substrate) and pretreatment process [10], [11]. The advantage of a metal substrate over silicon is its excellent electrical conductivity. Since CNTs can be directly grown on a metal substrate without external catalyst, the adherence between CNTs and substrate is greatly enhanced [12]. Furthermore, the synthesis of CNTs is easy to handle and process on metal substrates. In particular, the formation of holes on metal substrates can be easily achieved by simple acid etching treatments, thus enabling the formation of patterned field emitters. One of the major challenges in field emission is the screening effect, which arises when the spacing between CNTs is too small. Patterning of field emitters thus prevents the screening effect in field emission, consistent with many studies, which suggest that field emission properties of CNTs are strongly related to the shape of the emitter [13], [14]. This has necessitated the patterning of CNTs on metal substrates through photolithography in some studies [15].

In this article, instead of having to pattern the CNTs through photolithography, we explore the patterning of the metal alloy substrate into strips through a simple and inexpensive acid etching process. Given that the etching process is performed on the substrate before CNT growth, the CNTs are expected to be damage-free, and hence, exhibit better field emission properties compared to those in previous studies. To test the application of the stripe-patterned CNT emitters in X-ray imaging, we self-design and assemble an electron gun (*E*-gun) employing the stripe-patterned CNT emitters developed herein and capture an image of human teeth.

II. Experiment

CNTs were synthesized by thermal CVD (TCVD) on a metal alloy substrate, YEF-426, consisting of 42% nickel, 6% chromium, and 52% iron [Fig. 1(a)]. The strips that are 56-μm-wide with 142-μm spacing were achieved by acid etching with $FeCl_3$ [Fig. 1(b)]. Inside the chamber, the pressure was maintained at 10^{-6} torr to prevent oxidation, and the chamber was heated up to 900 °C. When the desired

Manuscript received August 19, 2019; revised September 18, 2019; accepted September 23, 2019. Date of publication October 17, 2019; date of current version November 27, 2019. This work was supported in part by the National Research Foundation of Korea (NRF) grants funded by the Korean Government (MSIP) under Grant NRF-2018M3A9E9024942. The review of this article was arranged by Editor M Blank. *(Corresponding author: Mallory Mativenga; Jehwang Ryu.)*

J. Lim, A. P. Gupta, S. J. Yeo, J. S. Ahn, and J. Ryu are with the Department of Physics, Kyung Hee University, Seoul 02447, South Korea (e-mail: jhryu@khu.ac.kr).

M. Mativenga is with the Department of Information Display, Kyung Hee University, Seoul 02447, South Korea (e-mail: mallory@tft.khu.ac.kr).

M. Kong is with the Department of Radiation Oncology, Kyung Hee University Medical Center, Kyung Hee University School of Medicine, Seoul 02447, South Korea.

C.-G. Cho is with CAT Beam Tech. Co. Ltd., Seoul 02455, South Korea.

S. H. Kim is with the Department of Radiology, Asan Medical Center, University of Ulsan College of Medicine, Seoul 05505, South Korea.

Color versions of one or more of the figures in this article are available online at http://ieeexplore.ieee.org.

Digital Object Identifier 10.1109/TED.2019.2943870

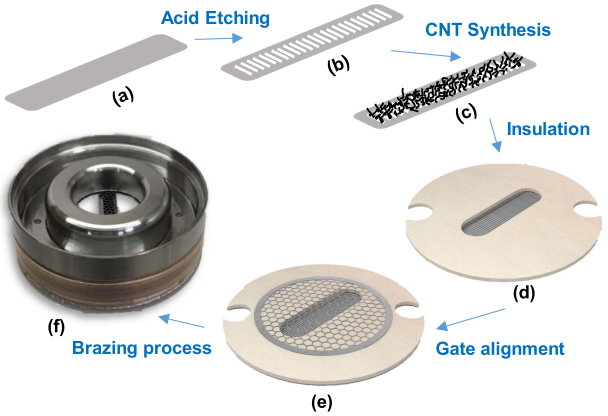

Fig. 1. Fabrication process of a CNT-based *E*-gun with the meshed gate electrode. (a) Un-patterned metal substrate. (b) Stripe-patterned substrate after acid etching. (c) Stripe-patterned-substrate/CNT stack after CNT growth. (d) Stripe-patterned-substrate/CNT/alumina-insulator stack. (e) Stripe-patterned-substrate/CNT/alumina-insulator/gate stack. (f) Completed *E*-gun after brazing.

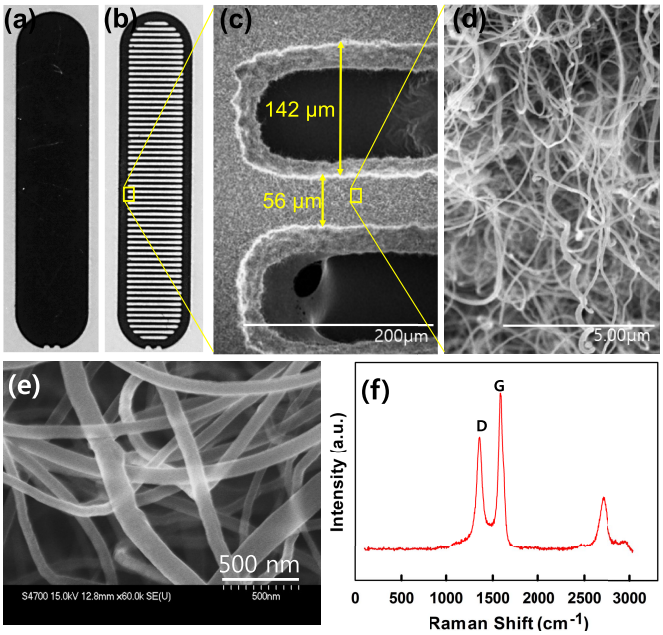

Fig. 2. Optical image of the fabricated (a) unpatterned and (b) stripe-patterned emitters. (c)–(e) SEM images of the stripe-patterned emitter grown on the metal substrate. (f) Raman spectrum.

temperature was reached, a pretreatment process was carried out with 70 sccm of NH_3 for 15 min at 7 torr. Finally, a mixture of 30 sccm of C_2H_2 and 70 sccm of NH_3 was inserted to grow the CNTs for 30 min. Evidence of CNT growth was examined through a scanning electron microscope (SEM). The synthesized unpatterned [Fig. 2(a)] and stripe-patterned [Fig. 2(b)] CNT emitters were assembled in a triode type *E*-gun structure with the help of an alumina insulator and gate mesh [Fig. 1(c)–(e)]. The anode was made of tungsten embedded on copper and biased within an anode voltage of 7 kV. The gate electrode had a hexagonal structure made up of Kovar plate that had 360 μm in diagonal and 100 μm in thickness. The *E*-gun structure had a 370-μm gate-to-cathode distance and a total emission area of 0.1377 cm^2.

A focuser was added to the *E*-gun for beam focusing through brazing at 850 °C under vacuum (10^{-7} torr). The high temperature was necessary because the filler used for joining the gate–cathode structure and focuser was AgCu, which has a melting point of about 850 °C. The completed *E*-gun is shown in Fig. 1(f). The details of the triode-type field emission measuring and X-ray generation system used herein are described elsewhere [16]. We used the open-type X-ray system with the stripe-patterned CNT emitters to obtain an X-ray image of human teeth by operating this system with an anode voltage of 60 kV. The operating anode current was 0.5 mA, and the vacuum inside the chamber was maintained at10^{-7} torr.

III. Results and Discussion

Fig. 2(c)–(e) shows the SEM images of synthesized CNTs at different magnifications. The CNTs exhibited the spaghetti-like orientation, with diameters ranging from 50–120 nm and an average length of about 5 μm. Due to the random existent of the catalyst on the metal surface, the CNTs were densely populated, nonuniform, and curved. This necessitated the performance of an aging process to eliminate long CNTs from the synthesized emitters [Fig. 2(d)], resulting in the improved uniformity in length. The field emission measurement was performed until the field emission characteristics became uniform. The Raman spectrum was characterized with *G*- and *D*-bands, respectively, located at 1593 and 1365 cm^{-1}, confirming the presence of multiwalled CNTs (MWCNTs) possessing the intensity ratio of the *D*- and *G*-bands (I_G/I_D) of 1.369 [Fig. 2(f)]. These results support the presence of minimum disorder in the synthesized CNTs. Moreover, the absence of the radial breathing mode (RBM) at values <500 cm^{-1} in the Raman spectrum is consistent with a multiwalled structure [17].

The cathode, on which the CNTs are grown, is inserted into a ceramic cover that ensures insulation from an external contact. Except for the emission area, the gap between the gate and emitter is covered with ceramic to reduce leakage current. For field emission measurements, the gate voltage is swept from 400 to 1300 V. A stability test was performed under the same conditions as those of the emission current measurement, but with the gate voltage fixed at 1.2 kV. This voltage was determined based on the gate voltage, which showed a value of 1.5 mA in the emission current measurement. Fig. 3 shows the comparison of the cathode currents of a stripe-patterned emitter and an unpatterned emitter after aging. For the aging process, ten preemission test measurements were performed, with a gate voltage sweep range of 400–1300 V. It is evident in Fig. 3 that the stripe-patterned emitter exhibited better emission characteristics compared to the unpatterned emitter. At 1.3 kV, the stripe-patterned emitter had an emission current of 2.32 mA, whereas the unpatterned emitter had only 0.22 mA, which is nearly a ten times difference. The turn-on voltage of the stripe-patterned emitter was also lower than that of the un-patterned emitter. By defining the turn-on voltage as the gate–voltage corresponding to an emission current of 10 μA/cm^2, the turn-on voltages were 600 and 800 V, respectively, for the former and latter.

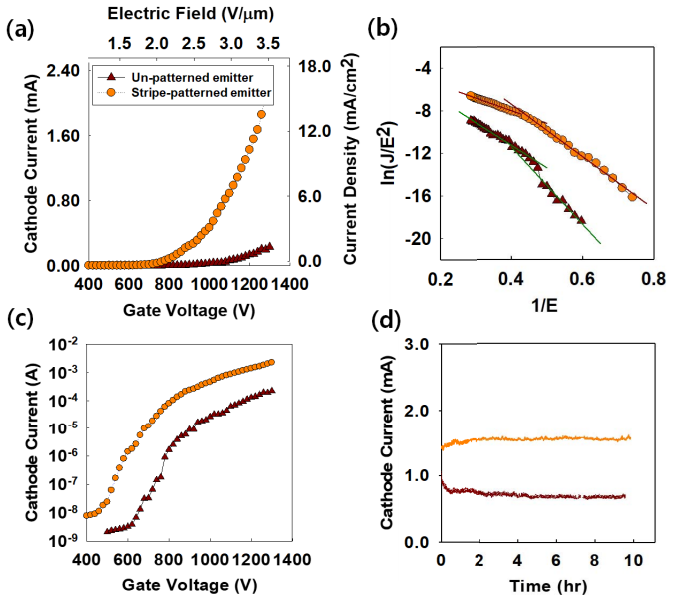

Fig. 3. Field emission characteristics of un-patterned and stripe-patterned emitters. (a) Current–voltage characteristics. (b) and (c) FN plot (b) and semilog plot (c) of the same data. (d) Stability test results.

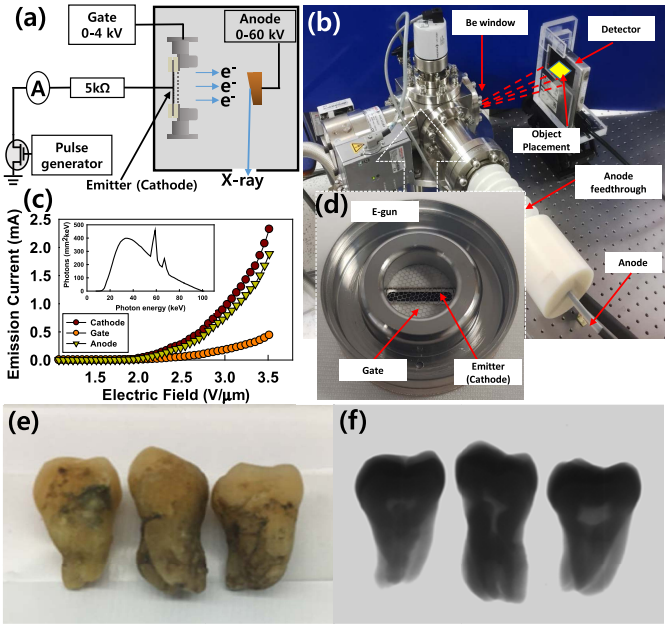

Fig. 4. (a) Schematic of the X-ray system. (b) Snapshot of the open-type X-ray system. (c) Triode-mode *I–V* characteristic of the stripe-patterned emitter and (inset) X-ray spectrum of the tungsten target with a beryllium filter. (d) *E*-gun employing stripe-patterned emitter. (e) Optical and (f) X-ray image of human teeth.

Given that the stripe-patterned emitter has a reduced effective emission area compared to the un-patterned emitter, it is expected to exhibit a lower field emission. However, the results of this article indicate that patterning of the emitter leads to a better field emission efficiency. The slope of the Fowler–Northeim (FN) plot is smaller for the striped-patterned emitter compared to the un-patterned emitter [Fig. 3(b)]. This implies that the field enhancement factor of the stripe-patterned emitter is larger than that of the un-patterned emitter. The field enhancement factor of stripe-patterned and un-patterned emitters was, respectively, 6034 and 3367. The slope change in the FN may be related to the change in the orientation of the CNTs, where the low and high electric fields, respectively, correspond to fields before and after the CNTs become erect.

In addition to the enhanced field emission, the stripe-patterned emitters also exhibited better operation stability [Fig. 3(d)]. During the first hour, the emission current of the stripe-patterned emitter increases gradually until it reaches 1.5 mA. The reason for this slight increase is not clear and warrants further investigation, but could also be due to a reorientation and stabilization period, where CNTs become erect along the direction of the electric field. When CNTs become erect, their distance from the gate decreases, and hence, field-emission increases. The process is reversible because repeated stability test measurements yield graphs with the same shape. Given that this phenomenon is not present in the unpatterned emitters, in which emission current continuously decreases with stress time [Fig. 3(d)], it could be related to the CNTs located at the edges in the stripe-patterned emitters.

Note that the emission current of the stripe-patterned emitter measured at 1.2 kV is higher than that of the un-patterned emitter measured at 1.8 kV. Higher field emission properties and better stability exhibited by the stripe-patterned emitters compared to the un-patterned emitters are related to the reduced screening effect (as a result of the spacing between strips) during field emission and enhanced edge effect (due to increased number of edges) [14], [15].

Note that the emission from CNTs at the edges is higher than that of CNTs at the center because of the former experience less screening effect and, thus, exhibit higher local electric fields. To verify the ability of the stripe-patterned CNT field emitters to generate X-rays, we designed and assembled an open-type X-ray system employing the *E*-gun with the striped patterned emitter (Fig. 4). Using the triode system [Fig. 4(a)], a cathode current of 0.644 mA and anode current of 0.522 mA were obtained at a gate electric field of 2.81 V/μm [Fig. 4(b)]. The anode current was measured by adjusting the gate electrode in the dc mode. The leakage current ratio was below 19%.

The X-ray image was taken at an anode accelerating voltage of 60 kV with the anode current of 0.5 mA achieved by applying a gate field of 2.75 V/μm for 0.1 s (single scan) in the open-type X-ray system [Fig. 4(c) and (d)]. The X-ray dose was approximately 10 mR for a focal spot size of 300 and 500 μm, respectively, for the vertical and horizontal axes [European Standard (EN 12543-5)] [18]. The simulated spectrum of the X-rays from the tungsten anode through the 0.2-mm-thick beryllium window is shown in the inset of Fig. 4(c) [19]. Note that a gate field of 5 V/μm had to be applied in our previous report to achieve the same anode current of 0.5 mA using un-patterned emitters [20]. We successfully took an X-ray image of human teeth using the X-ray system with stripe-patterned emitters as shown in Fig. 4(e) and (f). Given that the emission area (0.1377 cm^2) of the electron gun presented herein is exactly the same as the one in our previous report, stripe-patterning of emitters results in high emission current at low gate field and, hence, higher operational stability. This verifies the potential application

of the stripe-patterned emitters in the next-generation X-ray technology.

IV. Conclusion

We have demonstrated that CNT field emitters can be enhanced by growing the CNTs directly on stripe-patterned alloy substrates. The emission current increased tenfold, and the overall stability of the emitters improved by the use of the stripe-patterned substrate. The performance enhancement was attributed to the gaps between the strips, which resulted in the reduction of screening effects and the consequent decrease in edge effects. It can thus be predicted from this study that the field enhancement factor of an emitter is linked with the structure of the substrate. An E-gun implemented with the stripe-patterned substrate exhibited higher emission current at lower gate field compared to the E-gun implemented with the un-patterned substrate. Higher emission current at lower gate field implies higher operational stability, verifying the potential application of the stripe-patterned emitters in the next-generation X-ray sources.

References

[1] Z. Liu, G. Yang, Y. Z. Lee, D. Bordelon, J. Lu, and O. Zhou, "Carbon nanotube based microfocus field emission X-ray source for micro-computed tomography," *Appl. Phys. Lett.*, vol. 89, no. 10, Sep. 2006, Art. no. 103111. doi: 10.1063/1.2345829.

[2] Y. Xing *et al.*, "Design and realization of microwave frequency multiplier based on field emission from carbon nanotubes cold-cathode," *IEEE Trans. Electron Devices*, vol. 65, no. 3, pp. 1146–1150, Mar. 2018. doi: 10.1109/TED.2018.2793909.

[3] P. Zhang *et al.*, "Temperature comparison of looped and vertical carbon nanotube fibers during field emission," *Appl. Sci.*, vol. 8, no. 7, p. 1175, Jul. 2018. doi: 10.3390/app8071175.

[4] W. A. de Heer, A. Châtelain, and D. Ugarte, "A carbon nanotube field-emission electron source," *Science*, vol. 270, no. 5239, pp. 1179–1180, Nov. 1995. doi: 10.1126/science.270.5239.1179.

[5] C. R. Inscoe *et al.*, "Characterization and preliminary imaging evaluation of a clinical prototype stationary intraoral tomosynthesis system," *Med. Phys.*, vol. 45, no. 11, pp. 5172–5185, Oct. 2018. doi: 10.1002/mp.13214.

[6] X. Yuan *et al.*, "A truncated-cone carbon nanotube cold-cathode electron gun," *Carbon*, vol. 120, pp. 374–379, Mar. 2017. doi: 10.1016/j.carbon.2017.03.046.

[7] J.-T. Kang *et al.*, "Fast and stable operation of carbon nanotube field-emission X-ray tubes achieved using an advanced active-current control," *IEEE Electron Device Lett.*, vol. 36, no. 11, pp. 1209–1211, Nov. 2015. doi: 10.1109/LED.2015.2478157.

[8] S. Park *et al.*, "A fully closed nano-focus X-ray source with carbon nanotube field emitters," *IEEE Electron Device Lett.*, vol. 39, no. 12, pp. 1936–1939, Nov. 2018. doi: 10.1109/LED.2018.2873727.

[9] H. Kato, B. E. O'Rourke, and R. Suzuki, "Stable and high current density electron emission using coniferous carbon nano-structured emitter," *Diamond Rel. Mater.*, vol. 55, pp. 41–44, May 2015. doi: 10.1016/j.diamond.2015.03.001.

[10] P. Romero, R. Oro, M. Campos, J. M. Torralba, and R. G. de Villoria, "Simultaneous synthesis of vertically aligned carbon nanotubes and amorphous carbon thin films on stainless steel," *Carbon*, vol. 82, pp. 31–38, Feb. 2015. doi: 10.1016/j.carbon.2014.10.020.

[11] A. Castan *et al.*, "New method for the growth of single-walled carbon nanotubes from bimetallic nanoalloy catalysts based on Prussian blue analog precursors," *Carbon*, vol. 123, pp. 583–592, Oct. 2017. doi: 10.1016/j.carbon.2017.07.058.

[12] C. E. Baddour, F. Fadlallah, D. Nasuhoglu, R. Mitra, L. Vandsburger, and J.-L. Meunier, "A simple thermal CVD method for carbon nanotube synthesis on stainless steel 304 without the addition of an external catalyst," *Carbon*, vol. 47, no. 1, pp. 313–318, Jan. 2009. doi: 10.1016/j.carbon.2008.10.038.

[13] G. Chen *et al.*, "Low turn-on and uniform field emission from structurally engineered carbon nanotube arrays through growth on metal wire mesh substrates," *Mater. Res. Express*, vol. 4, no. 10, Oct. 2017, Art. no. 105041. doi: 10.1088/2053-1591/aa92f3.

[14] L. Nilsson *et al.*, "Scanning field emission from patterned carbon nanotube films," *Appl. Phys. Lett.*, vol. 76, no. 15, pp. 2071–2073, Apr. 2000. doi: 10.1063/1.126258.

[15] S. Fujii *et al.*, "Efficient field emission from an individual aligned carbon nanotube bundle enhanced by edge effect," *Appl. Phys. Lett.*, vol. 90, no. 15, Apr. 2007, Art. no. 153108. doi: 10.1063/1.2721876.

[16] A. P. Gupta *et al.*, "Direct synthesis of carbon nanotube field emitters on metal substrate for open-type X-ray source in medical imaging," *Materials*, vol. 10, no. 8, p. 878, Aug. 2017. doi: 10.3390/ma10080878.

[17] A. Sadezky, H. Muckenhuber, H. Grothe, R. Niessner, and U. Pöschl, "Raman microspectroscopy of soot and related carbonaceous materials: Spectral analysis and structural information," *Carbon*, vol. 43, no. 8, pp. 1731–1742, Jul. 2005. doi: 10.1016/j.carbon.2005.02.018.

[18] J. Ryu *et al.*, "Carbon nanotube field emission X-ray system for computed tomography," *Proc. SPIE*, vol. 8668, Mar. 2013, Art. no. 866860. doi: 10.1117/12.2007836.

[19] J. M. Boone, T. R. Fewell, and R. J. Jennings, "Molybdenum, rhodium, and tungsten anode spectral models using interpolating polynomials with application to mammography," *Med. Phys.*, vol. 24, no. 12, pp. 1863–1874, Dec. 1997. doi: 10.1118/1.598100.

[20] S. Park *et al.*, "Carbon nanotube field emitters synthesized on metal alloy substrate by PECVD for customized compact field emission devices to be used in X-ray source applications," *Nanomaterials*, vol. 8, no. 6, p. 378, 2018. doi: 10.3390/nano8060378.